

Nonlocal correlations in quantum energy teleportation: perspectives from their Majorana representations and information thermodynamics

Hiroaki Matsueda^{1,2}, Yusuke Masaki¹, Kanji Itoh¹, Atsushi Ono³, and Joji Nasu³

¹*Department of Applied Physics, Graduate School of Engineering, Tohoku University, Sendai 980-8579, Japan*

²*Center for Science and Innovation in Spintronics, Tohoku University, Sendai 980-8577, Japan*

³*Department of Physics, Graduate School of Science, Tohoku University, Sendai 980-8578, Japan*

(Dated: December 10, 2024)

Motivated by anomalous nonlocal correlation in the Kitaev spin liquids, we propose a quantum energy teleportation protocol between remote partners Alice and Bob on a quantum spin model, and examine how its performance is characterized by Majorana fermions that clearly depict nonlocal correlations inherent in the model. In our model, Bob's energy extraction is activated by local energy injection by Alice's projective measurement and subsequent classical communication of the measurement result. We derive two formulae: one for the maximally extracted energy by the protocol and the other for the maximum of energy reduction at Bob's local site. We find that the extracted energy becomes positive when a nonlocal correlator defined by Majorana fermions at Alice's and Bob's sites is finite. We also find that the amount of the energy reduction becomes positive when another nonlocal Majorana correlator is finite. In both formulae, the correlators appear as a result of Bob's feedback unitary operation. We discuss effective information-thermodynamical aspects behind the protocol at zero temperature.

I. INTRODUCTION

Quantum teleportation transfers quantum information (or a quantum state) to a distant place by using an entanglement pair and projective measurement. Quantum teleportation is thus the most fundamental protocol for quantum communication technologies, and nearly 30 years have passed since this protocol was developed [1]. Quantum teleportation provides meaningful perspectives not only in the field of communication technologies, but also in recent researches on traversable wormholes in spacetime physics and its holographic realization on quantum processors [2–5].

Phenomena similar to quantum teleportation can also be seen in solid-state physics, although the transportation range seems to be of microscopic scale. Nice playgrounds are Kitaev quantum spin systems. The Kitaev model is an exactly solvable quantum spin model, whose ground state is a quantum spin liquid with elementary excitations described by Majorana fermions [6–13]. Two related studies have been conducted in recent years. The first one is about detection of the magnetic moment at one edge of the Kitaev model after pulse magnetic excitation to the opposite edge [14–18]. The second one is about long-range correlation between two remote impurities introduced in the Kitaev model [19]. In both cases, there is no direct transportation of spin waves. Instead, the Majorana physics is a key for understanding such long-range correlations. In addition, performing braiding operations of Majorana zero modes is a candidate for teleportation-based quantum information processing [20–22]. Thus, the physics of Majorana fermions has good connection with quantum teleportation theories and technologies.

Unfortunately, the abovementioned two studies do not directly consider how each physical process and the long-range correlation correspond to traditional quantum tele-

portation protocols. In the protocol, any nonlocal correlation function between an information sender and receiver does not appear. In order to understand the roles of the Majorana correlations on the teleportation-like behaviors in the Kitaev systems, we consider quantum energy teleportation (QET) rather than quantum teleportation [23–32]. As shown later, this research is also related to a very fundamental question about the second law of information thermodynamics, which is how work extraction is enhanced by quantum information [33–39].

Motivated by these cross-disciplinary interests, we examine a QET protocol for remote partners Alice and Bob on the ground state of a one-dimensional quantum spin model that is transformed into a model of Majorana fermions. In a basic assumption of the QET protocol, Alice and Bob perform local operations and classical communication by a speed much faster than the transfer of any physical modes. Thus, this protocol does not demand direct physical connection between Alice and Bob except for the ground-state entanglement. In this situation, Bob's feedback unitary transformation activates energy extraction after local energy injection by Alice's projective measurement. We would like to understand how the entanglement (or nonlocal Majorana correlation) facilitates the positive energy extraction by the QET protocol. We will derive the formula to represent the relation between the extracted energy and a nonlocal Majorana correlator. We will also derive the formula that relates another nonlocal Majorana correlator to local energy reduction at Bob's site, and find that the result is consistent with our recent work on the upper bound on locally extractable energy from an entangled pure state under feedback control [39]. These nonlocal Majorana correlators appear as a result of Bob's feedback operation, and contribute to the energy extraction and the local energy reduction. If we interpret the extractable energy as work, it is a thermodynamically natural ques-

tion to ask whether the QET involves heat transfer between Bob's local system and the other part of the whole system. Even though we consider the QET protocol at zero temperature, it is possible to define heat as the difference between the amount of the local energy reduction and the work. The heat originates in the change in the interaction energy between the local system and the other part. We will find that the heat is finite in general and becomes zero for the QET process that maximizes the work. We will also mention the second law of effective information thermodynamics for Bob's local system in which the effective temperature originates in the entanglement between the local system and the other part of the whole system. We will find that the nonlocal Majorana correlator related to the local energy reduction is different from the quantum-classical (QC) mutual information appearing in our previous work [39], although both of the Majorana correlator and the QC-mutual information are quantum-information resources for driving these protocols.

This paper is organized as follows. In the next section, we introduce our model, and represent it using Jordan-Wigner fermions. In section III, we explain our QET protocol, and derive the formulae of the extracted energy and the local energy reduction. In section IV, we derive the Majorana fermion representations of these formulae, and discuss the roles of the nonlocal Majorana correlations on these formulae. Section V is devoted to the discussion about the first and second laws of effective information thermodynamics inherent in the present model. On the basis of the present result, we summarize our results in section VI. In Appendix A, the symmetry operations to determine the ground-state properties are provided. In Appendix B, mathematical details for deriving the maxima of the extracted energy and the local energy reduction are provided. In Appendix C, the effect of the degeneracy of even- and odd-parity states on the QET performance is provided. The derivations of some equations are also provided in Appendices D and E.

II. MODEL

The QET protocol is as follows: First, the ground state with quantum entanglement is prepared, and Alice makes a local measurement at one endpoint of the system. Next, the measurement result is transmitted to Bob, at the opposite endpoint, via a classical communication channel. Then, Bob performs a feedback unitary operation based on the result. Alice injects energy locally into the system by the measurement. Bob can extract energy from the system by the unitary operation. It is assumed that Alice's classical communication and Bob's manipulation are sufficiently faster than the transmission rate of elementary excitation that can occur after Alice's measurement.

Let us start with the Hamiltonian defined by

$$H = H_A + V + H_B, \quad (1)$$

$$H_A = h\sigma_A^z, \quad (2)$$

$$V = k(\sigma_A^x \sigma_{C_1}^x + \sigma_{C_1}^y \sigma_{C_2}^y + \sigma_{C_2}^x \sigma_B^x), \quad (3)$$

$$H_B = h\sigma_B^z, \quad (4)$$

where σ_i^α ($\alpha = x, y, z$) is the Pauli operator at site i (the site indices, A, C_1, C_2 , and B , are sometimes replaced with 0, 1, 2, and 3, respectively). The model contains four sites A, C_1, C_2 , and B , and their spatial geometry is illustrated in Fig. 1. The interaction strength k creates entanglement, and the edge magnetic field h controls the amount of the entanglement. The interaction term has a special form so that our model matches with the analysis of Majorana correlation in the Kitaev spin liquids. This point will be discussed in Sec. IV. We will apply the local operation and classical communication to this ground state.

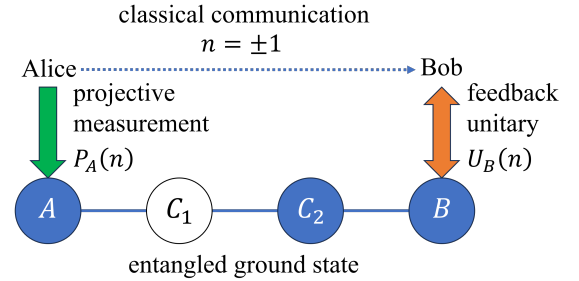


FIG. 1. Illustration of our four-spin model and protocol. Alice and Bob perform local projective measurement $P_A(n)$ to spin A and feedback unitary operation $U_B(n)$ to spin B , respectively. The green arrow at site A represents energy injection by the measurement, and the orange arrow at site B represents energy injection or extraction depending on the selection of the unitary operator. The classical communication between Alice and Bob is indicated by the dotted arrow, and the measurement results are $n = \pm 1$. The final result for the extracted energy is represented by the operators defined at sites A, C_2 , and B (blue shaded circles).

For later convenience to discuss Majorana correlation, we introduce the Jordan-Wigner transformation to spin operators:

$$\sigma_i^z = 2f_i^\dagger f_i - 1, \quad (5)$$

$$\sigma_i^x = \Theta_i(f_i^\dagger + f_i), \quad (6)$$

$$\sigma_i^y = -i\Theta_i(f_i^\dagger - f_i), \quad (7)$$

$$\Theta_i = e^{i\pi \sum_{l(<i)} f_l^\dagger f_l} = \prod_{l(<i)} (-\sigma_l^z), \quad (8)$$

where $i = 0, 1, 2, 3$ (A, C_1, C_2, B), f_i^\dagger and f_i are the creation and annihilation operators of the Jordan-Wigner fermion at site i , respectively, and Θ_i is the string operator ($\Theta_0 = 1$). Hereafter we abbreviate $\Theta_3 (= \Theta_B)$ as Θ .

The interaction term is transformed into

$$\begin{aligned}
 V = & k(f_A^\dagger - f_A)(f_{C_1}^\dagger + f_{C_1}) \\
 & - k(f_{C_1}^\dagger + f_{C_1})(f_{C_2}^\dagger - f_{C_2}) \\
 & + k(f_{C_2}^\dagger - f_{C_2})(f_B^\dagger + f_B).
 \end{aligned} \quad (9)$$

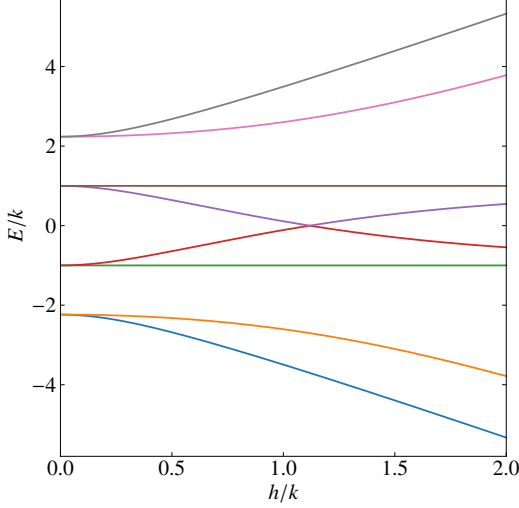


FIG. 2. Eigenvalue spectra E in the even-parity sector as a function of h . The lowest line represents the lowest value of ϵ in Eq. (15).

Figure 2 shows the h dependence of the eigenvalue spectra of H in the even-parity sector that is spanned by even numbers of Jordan-Wigner fermions. The eigenvalue spectra are degenerate with those in the odd-parity sector. We find symmetry between negative and positive spectra. We also find twofold degeneracies for all of the eigenstates in each parity sector for $h = 0$, and the degeneracies are lifted by introducing finite h values. In Appendix A, we summarize symmetry operations associated with these spectroscopic properties.

As a playground of QET, we prepare the lowest-energy eigenstate $|\psi\rangle$ in the even-parity sector. The state $|\psi\rangle$ for $h \geq 0$ is given by

$$\begin{aligned}
 |\psi\rangle = & Z[(|eeff\rangle + |fef\rangle) + \alpha(|ffff\rangle + |feef\rangle) \\
 & + (|ffee\rangle + |feef\rangle) + \beta(|eeee\rangle + |effe\rangle)], \quad (10)
 \end{aligned}$$

where $|eeff\rangle = f_{C_2}^\dagger f_B^\dagger |eeee\rangle$, $|eeee\rangle = |e\rangle_A \otimes |e\rangle_{C_1} \otimes |e\rangle_{C_2} \otimes |e\rangle_B$, $|eeee\rangle$ is the vacuum of the Jordan-Wigner fermions, and $\sigma_i^z |e\rangle_i = -|e\rangle_i$, $\sigma_i^z |f\rangle_i = |f\rangle_i$ with $i = A, C_1, C_2, B$. The parameters, α and β , are respectively defined by

$$\alpha = \frac{2k}{\epsilon + k - 2h}, \quad (11)$$

$$\beta = \frac{2k}{\epsilon + k + 2h}, \quad (12)$$

with the lowest energy $\epsilon = k(\alpha + \beta + 1)$, and the normalization factor Z is defined by

$$(4 + 2\alpha^2 + 2\beta^2) Z^2 = 1. \quad (13)$$

For α and β , we find the following equation:

$$k(\alpha - \beta) = 2h\alpha\beta. \quad (14)$$

Here, the lowest energy ϵ is determined by solving the following equation:

$$(\epsilon + k)(\epsilon^2 - 5k^2) - 4h^2(\epsilon - k) = 0. \quad (15)$$

We find that $\lim_{h \rightarrow 0} \epsilon = -\sqrt{5}k$ and $\epsilon < -\sqrt{5}k$ for $h > 0$ as shown in Fig. 2. By using Eqs. (11), (12), and (15), we can derive $\alpha\beta = (\epsilon - k)/(\epsilon + k) > 0$ for general h values. The expectation values of Hamiltonian terms H_A , V , and H_B by $|\psi\rangle$ are evaluated as

$$\epsilon = \epsilon_A + \epsilon_V + \epsilon_B, \quad (16)$$

$$\epsilon_A = \langle \psi | H_A | \psi \rangle = 2hZ^2(\alpha^2 - \beta^2) \leq 0, \quad (17)$$

$$\epsilon_V = \langle \psi | V | \psi \rangle = \epsilon - \epsilon_A - \epsilon_B = \epsilon - 2\epsilon_A, \quad (18)$$

$$\epsilon_B = \langle \psi | H_B | \psi \rangle = \epsilon_A. \quad (19)$$

For later convenience, we introduce the following representation for V : $V = H_L + H_C + H_R$, $H_L = k\sigma_A^x \sigma_{C_1}^x$, $H_C = k\sigma_{C_1}^y \sigma_{C_2}^y$, and $H_R = k\sigma_{C_2}^x \sigma_B^x$. The expectation values of H_L and H_R by $|\psi\rangle$ are given by

$$\epsilon_L = \langle \psi | H_L | \psi \rangle = 4kZ^2(\alpha + \beta) < 0, \quad (20)$$

$$\epsilon_R = \langle \psi | H_R | \psi \rangle = \epsilon_L. \quad (21)$$

For $h = 0$, $|\psi\rangle$ is factorized into the following form:

$$\begin{aligned}
 |\psi\rangle = & Z|fe - ef\rangle_{AB} \otimes |fe + ef\rangle_{C_1 C_2} \\
 & + Z\alpha|ff + ee\rangle_{AB} \otimes |ff + ee\rangle_{C_1 C_2}, \quad (22)
 \end{aligned}$$

where we have rearranged the order of the basis states and $|ff + ee\rangle_{AB} = |f\rangle_A \otimes |f\rangle_B + |e\rangle_A \otimes |e\rangle_B$. It is clear that the local states at Alice's and Bob's sites are correlated with each other. This correlation characterizes long-range entanglement in this model at least for $h = 0$.

III. PROTOCOL

Let us introduce Alice's measurement and Bob's feedback unitary operations in our QET protocol as already indicated in Fig. 1. Alice makes the following local measurements on spin A :

$$P_A(n) = \frac{1}{2}(I_A + n\vec{r} \cdot \vec{\sigma}_A), \quad (23)$$

$$\vec{r} = (r_x, r_y, r_z) = (\sin \mu \cos \nu, \sin \mu \sin \nu, \cos \mu), \quad (24)$$

where the measurement result n takes ± 1 , I_A is the identity operator, \vec{r} is a unit vector, and $P_A^2(n) = P_A(n)$.

Alice sends the measurement result n to Bob by the classical communication channel. Depending on the result n , Bob performs the following feedback unitary operation on spin B :

$$U_B(n) = e^{in\theta \vec{s} \cdot \vec{\sigma}_B} = I_B \cos \theta + in\vec{s} \cdot \vec{\sigma}_B \sin \theta, \quad (25)$$

$$\vec{s} = (s_x, s_y, s_z) = (\sin \xi \cos \eta, \sin \xi \sin \eta, \cos \xi), \quad (26)$$

where \vec{s} is a unit vector. For $\theta \neq 0, \pm\pi/2$, the feedback unitary operation is realized.

We evaluate the energy injected into Alice's local site by Alice's measurement, $\Delta E_A = E_A - \epsilon$, where E_A is the energy expectation value after Alice's measurement:

$$E_A = \sum_{n=\pm 1} \langle \psi | P_A(n) H P_A(n) | \psi \rangle. \quad (27)$$

Here, the quantum state after Alice's measurement is represented as $|\psi_A(n)\rangle = P_A(n) |\psi\rangle / \sqrt{\langle \psi | P_A(n) | \psi \rangle}$, and Eq. (27) is reduced to $E_A = \sum_{n=\pm 1} p_n \langle \psi_A(n) | H | \psi_A(n) \rangle$, where $p_n = \langle \psi | P_A(n) | \psi \rangle$ is the probability of obtaining a measurement result n . The energy E_A is evaluated as

$$\begin{aligned} E_A &= \sum_{n=\pm 1} \langle \psi | [P_A(n), H_A + H_L] P_A(n) | \psi \rangle + \epsilon \\ &= r_z^2 \epsilon_A + r_x^2 \epsilon_L + \epsilon_C + \epsilon_R + \epsilon_B, \end{aligned} \quad (28)$$

and the injected energy, ΔE_A , is given by

$$\Delta E_A = (r_z^2 - 1) \epsilon_A + (r_x^2 - 1) \epsilon_L. \quad (29)$$

It is clear that Alice's measurement injects positive energy ($\Delta E_A > 0$) into the local site A .

We also introduce the energy expectation value after Bob's feedback unitary operation:

$$E_B = \sum_{n=\pm 1} \langle \psi | P_A(n) U_B^\dagger(n) H U_B(n) P_A(n) | \psi \rangle, \quad (30)$$

which is evaluated as

$$\begin{aligned} E_B &= \sum_{n=\pm 1} \langle \psi | [P_A(n), H_A + H_L] P_A(n) | \psi \rangle + \epsilon_A + \epsilon_L + \epsilon_C \\ &\quad + \sum_{n=\pm 1} \langle \psi | P_A(n) U_B^\dagger(n) (H_R + H_B) U_B(n) | \psi \rangle \\ &= r_z^2 \epsilon_A + r_x^2 \epsilon_L + \epsilon_C \\ &\quad + \sum_{n=\pm 1} \langle \psi | P_A(n) U_B^\dagger(n) (H_B + H_R) U_B(n) | \psi \rangle. \end{aligned} \quad (31)$$

The extracted energy by Bob, $\Delta E_B = E_A - E_B$ (the energy extraction is possible for $\Delta E_B > 0$), is given by the sum of two contributions:

$$\Delta E_B = \Delta E_{B,B} + \Delta E_{B,R}, \quad (32)$$

where

$$\Delta E_{B,i} = \epsilon_i - \sum_{n=\pm 1} \langle \psi | P_A(n) U_B^\dagger(n) H_i U_B(n) | \psi \rangle, \quad (33)$$

with $i = B, R$. The quantity $\Delta E_{B,B}$ corresponds to the reduction of internal energy of Bob's local system. We have confirmed that Eqs. (32) and (33) hold regardless of the details of H_C under the constraint that H_C does not contain the operators defined at sites A , C_2 , and B , since ϵ_C disappears by subtracting E_A and E_B . The second term of $\Delta E_{B,i}$ corresponds to nonlocal correlation between Alice's measurement operator $P_A(n)$ and the operator $U_B^\dagger(n) H_i U_B(n)$ that is associated with Bob's feedback operation. The quantities $\Delta E_{B,B}$ and $\Delta E_{B,R}$ are evaluated as follows:

$$\begin{aligned} \Delta E_{B,B} &= \epsilon_B (1 - s_z^2) (1 - \cos(2\theta)) \\ &\quad - h (r_x s_y C_{AB} - r_y s_x D_{AB}) \sin(2\theta), \end{aligned} \quad (34)$$

$$\begin{aligned} \Delta E_{B,R} &= \epsilon_R (1 - s_x^2) (1 - \cos(2\theta)) \\ &\quad + k r_x s_y C_{AR} \sin(2\theta), \end{aligned} \quad (35)$$

where the correlators, C_{AB} , D_{AB} , and C_{AR} are, respectively, defined by

$$C_{AB} = \langle \psi | \sigma_A^x \sigma_B^x | \psi \rangle = 4Z^2 (1 + \alpha\beta), \quad (36)$$

$$D_{AB} = \langle \psi | \sigma_A^y \sigma_B^y | \psi \rangle = 4Z^2 (1 - \alpha\beta), \quad (37)$$

$$C_{AR} = \langle \psi | \sigma_A^x \sigma_{C_2}^x \sigma_B^z | \psi \rangle = 4Z^2 (\alpha - \beta). \quad (38)$$

For $h \rightarrow 0$ ($\alpha = \beta$ and $\alpha\beta = (3 + \sqrt{5})/2 > 1$), we find $C_{AB} = 1$, $D_{AB} < 0$, and $C_{AR} = 0$. In order to achieve $\Delta E_B = \Delta E_{B,B} + \Delta E_{B,R} > 0$, at least either $\Delta E_{B,B}$ or $\Delta E_{B,R}$ must be positive. Since the first terms in Eqs. (34) and (35) are always negative, their second terms are essential to $\Delta E_B > 0$. The second terms are finite values for the feedback operation ($\theta \neq 0, \pm\pi/2$), at which non-local correlations C_{AB} , D_{AB} , and C_{AR} appear.

If we replace $U_B(n)$ with an unitary operation without feedback, u_B ($= U_B(+1)$ or $U_B(-1)$), in Eq. (33), we find

$$\begin{aligned} \epsilon_B - \sum_{n=\pm 1} \langle \psi | P_A(n) u_B^\dagger H_B u_B | \psi \rangle \\ = \epsilon_B (1 - s_z^2) (1 - \cos(2\theta)), \end{aligned} \quad (39)$$

$$\begin{aligned} \epsilon_R - \sum_{n=\pm 1} \langle \psi | P_A(n) u_B^\dagger H_R u_B | \psi \rangle \\ = \epsilon_R (1 - s_x^2) (1 - \cos(2\theta)). \end{aligned} \quad (40)$$

Here, the absence of n dependence of u_B leads to cancellation of the effect of Alice's measurement $\sum_n P_A(n) = 1$. The results support our statement that the feedback control induces the effects of the nonlocal correlations on $\Delta E_{B,B}$ and $\Delta E_{B,R}$.

By optimizing \vec{r} , \vec{s} , and θ (see Appendix B), we obtain the maximum of ΔE_B , denoted by ΔE_B^{\max} , as

$$\Delta E_B^{\max} = \sqrt{\epsilon_B^2 + (h D_{AB})^2} - |\epsilon_B|, \quad (41)$$

where the optimization conditions are given by

$$\vec{r} = (0, 1, 0), \quad (42)$$

$$\vec{s} = (1, 0, 0), \quad (43)$$

$$\sin(2\theta) = \frac{hD_{AB}}{\sqrt{\epsilon_B^2 + (hD_{AB})^2}}, \quad (44)$$

$$\cos(2\theta) = \frac{-\epsilon_B}{\sqrt{\epsilon_B^2 + (hD_{AB})^2}}. \quad (45)$$

For the parameters that maximize ΔE_B , we find that $\Delta E_{B,B}$ is equal to $\Delta E_{B,B}^{\max}$ and $\Delta E_{B,R}$ becomes zero:

$$\Delta E_{B,B} = \epsilon_B + \sqrt{\epsilon_B^2 + (hD_{AB})^2} = \Delta E_{B,B}^{\max}, \quad (46)$$

$$\Delta E_{B,R} = 0. \quad (47)$$

These results show that a part of the second term in Eq. (34), $hr_y s_x D_{AB} \sin(2\theta)$, is crucial for the positive energy extraction.

We also derive the maximum value of $\Delta E_{B,B}$, denoted by $\Delta E_{B,B}^{\max}$, which is a primary focus in our previous study [39] (see Appendix B). The maximum value is obtained as

$$\Delta E_{B,B}^{\max} = \sqrt{\epsilon_B^2 + (hC_{AB})^2} - |\epsilon_B|, \quad (48)$$

where the optimization conditions are given by

$$\vec{r} = (1, 0, 0), \quad (49)$$

$$\vec{s} = (0, 1, 0), \quad (50)$$

$$\sin(2\theta) = \frac{-hC_{AB}}{\sqrt{\epsilon_B^2 + (hC_{AB})^2}}, \quad (51)$$

$$\cos(2\theta) = \frac{-\epsilon_B}{\sqrt{\epsilon_B^2 + (hC_{AB})^2}}. \quad (52)$$

For the parameters that maximize $\Delta E_{B,B}$, we find that $\Delta E_{B,R}$ is always negative:

$$\Delta E_{B,R} = \epsilon_R (1 - \cos(2\theta)) + kC_{AR} \sin(2\theta) < 0. \quad (53)$$

Because of the inequality $|C_{AB}| > |D_{AB}|$, $\Delta E_{B,B}^{\max}$ is larger than ΔE_B^{\max} . However, because of the negative feature of $\Delta E_{B,R}$, the maximum of ΔE_B can not be reached by optimizing $\Delta E_{B,B}$.

Figure 3(a) shows the h dependence of D_{AB} and C_{AB} , which are crucial factors for positive $\Delta E_{B,B}^{\max}$ and $\Delta E_{B,B}^{\max}$, respectively, as already shown in Eqs. (41) and (48). These correlators are large for a small- h region. Their behaviors after multiplying h show only weak- h dependence except for the small- h region. Figure 3(b) shows ΔE_A for $\vec{r} = (0, 1, 0)$ and $\vec{r} = (1, 0, 0)$, corresponding to ΔE_B^{\max} and $\Delta E_{B,B}^{\max}$, respectively, as a function of h . We first examine the h dependence of ΔE_A . The local energy change by the projection measurement is mediated by the Alice's local Hamiltonian H_A . It is natural that ΔE_A increases as h increases. We next examine the h dependence of ΔE_B^{\max} and $\Delta E_{B,B}^{\max}$. Both of them are

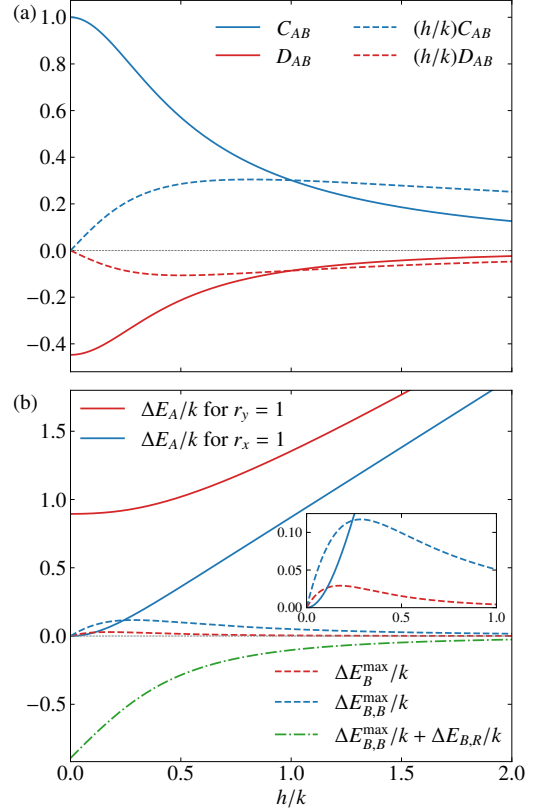


FIG. 3. (a) Nonlocal correlators C_{AB} and D_{AB} (hC_{AB} and hD_{AB}) as a function of h . (b) ΔE_A for $r_y = 1$, ΔE_A for $r_x = 1$, ΔE_B^{\max} , $\Delta E_{B,B}^{\max}$, and the sum of Eq. (48) and Eq. (53), as a function of h . The inset shows a magnified view for $h < k$.

zero for $h = 0$, and start to increase with h . Further increase of h reduces their magnitudes, because the effect of hD_{AB} and hC_{AB} on ΔE_B^{\max} and $\Delta E_{B,B}^{\max}$ is smeared out by the increase of $|\epsilon_B|$ in large- h region. We find $\Delta E_A > \Delta E_{B,B}^{\max}$ for $r_y = 1$. The ratio, $\Delta E_B^{\max}/\Delta E_A$ is about 0.032 for $h = 0.18k$ that is a peak position of ΔE_B^{\max} . We also find $\Delta E_A > \Delta E_{B,B}^{\max}$ for $r_x = 1$ and $h > 0.24k$. The inequality is reversed for $h < 0.24k$. We plot ΔE_B as the green dash-dotted line in Fig. 3(b) when $\Delta E_{B,B}$ is maximized. This quantity is given by the sum of Eqs. (48) and (53). We find that the quantity is negative and $|\Delta E_{B,R}| \gg \Delta E_{B,B}^{\max}$. Therefore, even if the amount of reduction in the internal energy for $h < 0.24k$ is greater than the amount of energy injected into the system, the work to be taken out of the system does not exceed the amount of energy injected.

IV. MAJORANA FERMION REPRESENTATION OF NONLOCAL CORRELATORS

Our main purpose of this paper is to convert the present QET model into a Majorana fermion model so

that we examine relationship between QET and Majorana nonlocal correlation. The conversion is realized by introducing the following Majorana representation:

$$b_l = f_l^\dagger + f_l, \quad (54)$$

$$c_l = i(f_l^\dagger - f_l), \quad (55)$$

$$c_m = f_m^\dagger + f_m, \quad (56)$$

$$b_m = i(f_m^\dagger - f_m), \quad (57)$$

for $l = A, C_2$ and $m = C_1, B$. Then, the QET Hamiltonian is mapped onto the following form:

$$H = i h b_A c_A - i k (c_A c_{C_1} - c_{C_1} c_{C_2} + c_{C_2} c_B) + i h c_B b_B. \quad (58)$$

For $h = 0$, the Hamiltonian is described by the bilinear form of itinerant c -Majorana fermions, and b -Majorana fermions are zero modes. The introduction of a finite h value induces coupling between c - and b -Majorana fermions at both edges. Let us compare this model with the conventional Kitaev model defined on a two-dimensional honeycomb lattice: $H = \sum_{\langle i, j \rangle_a} J_a \sigma_i^a \sigma_j^a$, where $\langle i, j \rangle_a$ represents the sum over nearest-neighbor pairs connected by an a -bond (each vertex in the honeycomb lattice has three bonds, and we label them $a = x, y, z$). By the transformation $\sigma_j^a = i b_j^a c_j$, the Hamiltonian is mapped onto an itinerant c -Majorana fermion system coupled to Z_2 gauge fields $u_{ij}^a = i b_i^a b_j^a$. The introduction of magnetic field induces coupling between b - and c -Majorana fermions. Although the transformation from spin operators to Majorana operators in our model is different from that in the Kitaev model, a correspondence between these two models can be observed as follows: the Majorana hopping with J_a in the Kitaev model corresponds to the k term in Eq. (58). The Zeeman-field term in the Kitaev model is usually represented as $-\sum_a h_a \sigma_j^a = -\sum_a h_a b_j^a c_j$ at site j , and this representation corresponds to the edge-field term in Eq. (58). Thus, our model can be viewed as one-dimensional simplification of the Kitaev model with edge magnetic fields [14–18]. In the previous work [19], the Kitaev model with two vacancies under a magnetic field is examined. In this case also, the b - c hopping terms of the nearest-neighbor sites of the vacancies appear, when we treat the magnetic field perturbatively.

We focus on the Majorana correlation, $\langle \psi | i b_A b_B | \psi \rangle$, that is evaluated as

$$\langle \psi | i b_A b_B | \psi \rangle = -4Z^2 (1 + \alpha\beta), \quad (59)$$

which reminds us of C_{AB} in Eq. (36). In order to clarify the reason for their equivalence except for the sign, the operator product $i b_A b_B$ before taking the expectation value is evaluated as

$$i b_A b_B = \sigma_A^x (\sigma_A^z \sigma_{C_1}^z \sigma_{C_2}^z) (i \sigma_B^y) = \sigma_A^x \sigma_B^x (-P), \quad (60)$$

where $P (= \sigma_A^z \sigma_{C_1}^z \sigma_{C_2}^z \sigma_B^z)$ is the parity operator. For the even-parity state $|\psi\rangle$ ($P|\psi\rangle = |\psi\rangle$), we actually obtain

$$\langle \psi | i b_A b_B | \psi \rangle = \langle \psi | \sigma_A^x \sigma_B^x (-1) | \psi \rangle = -C_{AB}. \quad (61)$$

For the odd-parity sector, see Appendix C. We also consider the Majorana representation of D_{AB} and C_{AR} . The results are given by

$$D_{AB} = \langle \psi | i c_A c_B P | \psi \rangle = \langle \psi | i c_A c_B | \psi \rangle, \quad (62)$$

$$C_{AR} = \langle \psi | i b_A c_{C_2} P | \psi \rangle = \langle \psi | i b_A c_{C_2} | \psi \rangle. \quad (63)$$

The quantity C_{AB} (D_{AB}) represents correlation between the b -Majorana (c -Majorana) fermions at both edges. These correlators, C_{AB} and D_{AB} , appear as a result of feedback control after classical communication between Alice and Bob, and are important for maximizing $\Delta E_{B,B}$ and ΔE_B , respectively. On the other hand, the correlator C_{AR} in $\Delta E_{B,R}$ is less important for the energy extraction. In particular, $\Delta E_{B,R}$ disappears for the maximization of ΔE_B . The Majorana representation of C_{AR} does not contain information about Majorana fermions at Bob's site, even though the original representation in Eq. (37) contains the spin operator σ_B^z at Bob's site. Therefore, we consider that the Majorana representation is a nice benchmark of how the communication between Alice and Bob is reflected to the maximum energy extraction and the maximum local-energy reduction.

V. ON THE FIRST AND SECOND LAWS OF EFFECTIVE INFORMATION THERMODYNAMICS

Let us discuss effective information-thermodynamical aspects behind the present QET model. Equation (32) is suggestive for considering the heat transfer that inevitably occurs in the QET process. The quantity ΔE_B is work that is taken out of the whole four-site system by Bob's local feedback control. Let us denote the work that Bob's local system gets as $W = -\Delta E_B$ and the increase in the internal energy of Bob's local system as $\Delta U = -\Delta E_{B,B}$. Then, Eq. (32) is reduced to the first law of effective thermodynamics for Bob's local system, $W + Q = \Delta U$, where Q is the heat absorbed by Bob's local system and assigned as

$$Q = \Delta E_{B,R}. \quad (64)$$

For the negative $\Delta E_{B,R}$, heat is necessarily released to the outside of Bob's local system through the interaction term H_R . A special case is maximization of ΔE_B , in which the heat transfer does not occur.

Equation (34) (or (48)) reminds us of the upper bound of work extraction in the second law of information thermodynamics, since the nonlocal correlator C_{AB} , quantum information in the ground state, is a crucial source for maximizing $\Delta E_{B,B}$. However, the nonlocal correlator is different from the QC-mutual information that is a resource of the work extraction. In this section, we discuss their difference.

The second law is usually defined for isothermal processes at temperature T , and is given by $W_{\text{ext}} \leq -\Delta F + T I_{\text{QC}}$, where the upper bound of the work extraction

W_{ext} contains information-gain term characterized by the QC-mutual information I_{QC} as well as free-energy change ΔF [33, 40, 41]. Motivated by the second law, some of the present authors have recently derived the upper bound on locally extractable energy from entangled pure states under feedback control [39]. The present setup matches with that of Ref. [39], when we regard H_B as the Hamiltonian of the local system of our interest (in Ref. [39], we did not consider interaction terms and there is no heat transfer, even if we consider the maximization of $\Delta E_{B,B}$). The energy reduction $\Delta E_{B,B}$ shows the second-law-like behavior as

$$\Delta E_{B,B} \leq \mathcal{F}(\rho_B^i; H_B) - F(\sigma_B) + \frac{1}{\beta_{\text{eff}}} I_{\text{QC}}, \quad (65)$$

where $\mathcal{F}(\rho_B^i; H_B)$ is the nonequilibrium free energy for the reduced density matrix of the ground state $\rho_B^i = \text{tr}_{AC_1C_2} |\psi\rangle \langle \psi|$, $F(\sigma_B)$ is the free energy of the thermal equilibrium state for the local Hamiltonian H_B , $\sigma_B = e^{-\beta_{\text{eff}} H_B} / Z_{\text{eff}}$ with the partition function Z_{eff} , and β_{eff} is an effective inverse temperature that originates in the coupling between B site and C_1C_2 sites. Two important quantities in Eq. (65) are the free-energy difference and the QC-mutual information, I_{QC} , respectively defined by

$$\mathcal{F}(\rho_B^i; H_B) - F(\sigma_B) = \frac{1}{\beta_{\text{eff}}} D(\rho_B^i \| \sigma_B) \geq 0, \quad (66)$$

$$I_{\text{QC}} = S(\rho_B^i) - \sum_{n=\pm 1} p_n S(\rho_B^m(n)) \geq 0, \quad (67)$$

where $D(\rho_B^i \| \sigma_B) = \text{tr}_B (\rho_B^i \log(\rho_B^i / \sigma_B))$ denoting the Kullback-Leibler (KL) divergence, $S(\sigma) = -\text{tr}_B (\sigma \log \sigma)$ denoting the von Neumann entropy of a density matrix σ , and $\rho_B^m(n) = \text{tr}_{AC_1C_2} |\psi_A(n)\rangle \langle \psi_A(n)|$. The KL divergence shows how the initial nonequilibrium state is far from σ_B , and is also an important resource of the energy reduction as well as the QC-mutual information. The equality condition of Eq. (65) holds only if the following relation is satisfied:

$$S(\sigma_B) = \min_{\{P_A(n)\}} \sum_n p_n S(\rho_B^m(n)), \quad (68)$$

where the minimization is performed over all possible projection operators, and is realized for $\vec{r} = (1, 0, 0)$ (see Appendix D). The projection operator $P_A(n)$ for the minimization also gives the maximum value of $\Delta E_{B,B}$ in the present case. Equation (68) is used for the determination of β_{eff} .

As shown in Appendix E, the right-hand side (RHS) of Eq. (65) becomes equivalent to $\Delta E_{B,B}^{\text{max}}$ in Eq. (48) for β_{eff} determined by Eq. (68). According to Eq. (34), $\Delta E_{B,B}^{\text{max}}$ is the sum of $\epsilon_B (1 - \cos(2\theta))$ and $-hC_{AB} \sin(2\theta)$ with Eqs. (51) and (52). The former contribution, $\epsilon_B (1 - \cos(2\theta))$, is always negative, and then the latter contribution, $-hC_{AB} \sin(2\theta)$ is larger than the RHS of Eq. (65). The KL divergence contains information about entanglement-entropy change by the measurement, and

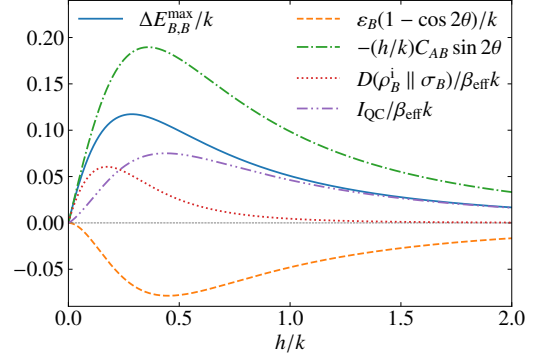


FIG. 4. $\Delta E_{B,B}^{\text{max}}$, $\epsilon_B (1 - \cos(2\theta))$, $-hC_{AB} \sin(2\theta)$, $D(\rho_B^i \| \sigma_B) / \beta_{\text{eff}}$, and $I_{\text{QC}} / \beta_{\text{eff}}$ as a function of h . The trigonometric functions are defined by Eqs. (51) and (52).

thus not only the QC-mutual information but also the KL divergence is related to C_{AB} .

Figure 4 shows the h dependence of all components in $\Delta E_{B,B}^{\text{max}}$ and the RHS of Eq. (65). We actually observe $-hC_{AB} \sin(2\theta) \geq \Delta E_{B,B}^{\text{max}} = (D(\rho_B^i \| \sigma_B) + I_{\text{QC}}) / \beta_{\text{eff}}$. As h increases, $D(\rho_B^i \| \sigma_B) / \beta_{\text{eff}}$ tends to disappear. The decay of $D(\rho_B^i \| \sigma_B) / \beta_{\text{eff}}$ is more remarkable than that of $I_{\text{QC}} / \beta_{\text{eff}}$. For $h/k > 1$, the RHS of Eq. (65) is almost equal to $I_{\text{QC}} / \beta_{\text{eff}}$. In this parameter region, $\epsilon_B (1 - \cos(2\theta))$ still remains, and this decay is slow. These data show that the nonlocal correlation term is not simply equal to the QC-mutual information even for the parameter region in which the KL divergence disappears.

VI. CONCLUDING REMARKS

We have considered QET on a quantum spin model and its Majorana representation in order to examine the roles of the Majorana correlations on the teleportation properties. We have derived the formula for connecting the maximally extracted energy ΔE_B^{max} with the nonlocal c -Majorana correlator D_{AB} , and have shown that the correlator is necessary for the positive energy extraction. We have also derived the formula about the maximum of the local energy reduction $\Delta E_{B,B}^{\text{max}}$ that is consistent with our previous work [39]. In this case, the nonlocal b -Majorana correlator C_{AB} is necessary for the energy reduction. In both cases, the nonlocal correlators appear as a result of Bob's feedback control. We have assigned $\Delta E_{B,R}$ as an effective heat absorption by the local system. We have found that there is no heat transfer when the extracted energy is maximized. We have also found that the Majorana correlator C_{AB} is different from the QC-mutual information in our previous work [39], although both of the Majorana correlator and the QC-mutual information are quantum-information resources for driving these protocols.

Equations (32) and (33) hold regardless of the details of H_C , although the values of C_{AB} , D_{AB} , and C_{AR} depend on the system size L . Thus, our statements are applicable to larger systems and systems with different geometries and spatial dimension. We have numerically evaluated those correlators for $H_C = -ik \sum_{l=0}^{L-2} (-1)^l c_l c_{l+1}$ up to $L = 1000$ in one dimension. For various L values, we have found that $C_{AB} = 1$ for $h = 0$ and C_{AB} decreases with increasing h (see also Fig. 3(a) for $L = 4$). With increasing L , the decrease becomes stronger. For various L values, we have also found that the absolute value of D_{AB} is maximum for $h = 0$ and decreases with increasing

h (see also Fig. 3(a) for $L = 4$). The absolute value shows power-law decay as a function of L for finite- h values, which is an evidence of quantum criticality of our model. The slow decay due to the power-law correlation enables us to consider QET for relatively large- L systems.

In the previous study of the Kitaev model [14], the induced magnetic moment after the pulse field excitation is measured by the time-dependent calculation. The time delay of the classical communication in the QET protocol may weaken the QET performance. It is a future work whether our statement holds in time-dependent cases.

This work was supported by JSPS KAKENHI Grant Numbers JP24K06878, JP24K00563, JP24K02948, JP23K22492, and CSIS in Tohoku University.

-
- [1] C. H. Bennett, G. Brassard, C. Crepeau, R. Jozsa, A. Peres, and W. K. Wootters., Phys. Rev. Lett. **70**, 1895 (1993).
- [2] L. Susskind and Y. Zhao, Phys. Rev. D **98**, 046016 (2018).
- [3] T. Schuster, B. Kobrin, P. Gao, I. Cong, E. T. Khabiboulline, N. M. Linke, M. D. Lukin, C. Monroe, B. Yoshida, and N. Y. Yao., Phys. Rev. X **12**, 031013 (2022).
- [4] D. Jafferis, A. Zlokapa, J. D. Lykken, D. K. Kolchmeyer, S. I. Davis, N. Lauk, H. Neven, M. Spiropulu., Nature **612**, 51 (2022).
- [5] A. Milekhin and F. K. Popov, arXiv:2210.03083.
- [6] A. Kitaev, Ann. Phys. (NY) **321**, 2 (2006).
- [7] Z. Nussinov and J. van den Brink, Rev. Mod. Phys. **87**, 1 (2015).
- [8] M. Hermanns, I. Kimchi, and J. Knolle, Annu. Rev. Condens. Matter Phys. **9**, 17 (2018).
- [9] J. Knolle and R. Moessner, Annu. Rev. Condens. Matter Phys. **10**, 451 (2019).
- [10] H. Takagi, T. Takayama, G. Jackeli, G. Khaliullin, and S. E. Nagler, Nat. Rev. Phys. **1**, 264 (2019).
- [11] L. Janssen and M. Vojta, J. Phys.: Condens. Matter **31**, 423002 (2019).
- [12] Y. Motome and J. Nasu, J. Phys. Soc. Jpn. **89**, 012002 (2020).
- [13] C. Hickey and S. Trebst, Phys. Rep. **950**, 1 (2022).
- [14] T. Minakawa, Y. Murakami, A. Koga, and J. Nasu, Phys. Rev. Lett. **125**, 047204 (2020).
- [15] A. Koga, Y. Murakami, and J. Nasu, Phys. Rev. B **103**, 214421 (2021).
- [16] H. Taguchi, Y. Murakami, A. Koga, and J. Nasu, Phys. Rev. B **104**, 125139 (2021).
- [17] J. Nasu, Y. Murakami, and A. Koga, Phys. Rev. B **106**, 024411 (2022).
- [18] T. Misawa, J. Nasu, and Y. Motome, Phys. Rev. B **108**, 115117 (2023).
- [19] M. O. Takahashi, M. G. Yamada, M. Udagawa, T. Mizushima, S. Fujimoto., Phys. Rev. Lett. **131**, 236701 (2023).
- [20] S. Vijay and L. Fu, Phys. Rev. B **94**, 235446 (2016).
- [21] L. Fu, Phys. Rev. Lett. **104**, 056402 (2010).
- [22] H.-L. Huang, M. Narozniak, F. Liang, Y. Zhao, A. D. Castellano, M. Gong, Y. Wu, S. Wang, J. Lin, Y. Xu, H. Deng, H. Rong, J. P. Dowling, C.-Z. Peng, T. Byrnes, X. Zhu, and J.-W. Pan, Phys. Rev. Lett. **126**, 090502 (2021).
- [23] M. Hotta, Phys. Lett. A **372**, 5671 (2008).
- [24] M. Hotta, Phys. Rev. D **78**, 045006 (2008).
- [25] M. Hotta, J. Phys. Soc. Jpn. **78**, 034001 (2009).
- [26] M. Hotta, Phys. Lett. A **374**, 3416 (2010).
- [27] J. Trevison and M. Hotta, J. Phys. A: Math. Theor. **48**, 175302 (2015).
- [28] N. A. Rodriguez-Briones, H. Katiyar, E. Martinez-Martinez, and R. Laflamme., Phys. Rev. Lett. **130**, 110801 (2023).
- [29] K. Ikeda, Phys. Rev. Appl. **20**, 024051 (2023).
- [30] K. Ikeda, AVS Quantum Sci. **5**, 035002 (2023).
- [31] K. Itoh, Y. Masaki, and H. Matsueda, arXiv:2305.03967.
- [32] J. Wang and S. Yao, arXiv:2405.13886.
- [33] T. Sagawa and M. Ueda, Phys. Rev. Lett. **100**, 080403 (2008).
- [34] H. Tajima, Phys. Rev. E **88**, 042143 (2013).
- [35] K. Funo, Y. Watanabe, and M. Ueda, Phys. Rev. A **88**, 052319 (2013).
- [36] J. J. Park, K.-H. Kim, T. Sagawa, and S. W. Kim, Phys. Rev. Lett. **111**, 230402 (2013).
- [37] G. Manzano, F. Plastina, and R. Zambrini, Phys. Rev. Lett. **121**, 120602 (2018).
- [38] S. Minagawa, M. H. Mohammad, K. Sakai, K. Kato, and F. Buscemi, arXiv:2308.15558.
- [39] K. Itoh, Y. Masaki, and H. Matsueda, arXiv:2408.11522.
- [40] H. J. Groenewold, Int. J. Theor. Phys. **4**, 327 (1971).
- [41] M. Ozawa, J. Math. Phys. **27**, 759 (1986).

Appendix A: Symmetry operations

The eigenstates of our model can be characterized by various operators commuting or anticommuting with the Hamiltonian. We define the following four operators:

$$P = \sigma_A^z \sigma_{C_1}^z \sigma_{C_2}^z \sigma_B^z, \quad (\text{A1})$$

$$Q = \sigma_A^z \sigma_{C_1}^z \sigma_{C_2}^x, \quad (\text{A2})$$

$$R = \sigma_{C_1}^x \sigma_{C_2}^x, \quad (\text{A3})$$

$$S = \sigma_A^x \sigma_{C_1}^y \sigma_{C_2}^x \sigma_B^y, \quad (\text{A4})$$

where we find $[P, H] = 0$, $[Q, H] = 0$, $\{P, Q\} = 0$, $[R, H] = 0$, $[R, P] = 0$, $\{R, Q\} = 0$, $\{S, H\} = 0$, $[P, S] = 0$, $P^2 = 1$, $Q^2 = 1$, $R^2 = 1$, and $S^2 = 1$. The operator P is the parity operator for the number of Jordan-Wigner fermions with eigenvalues ± 1 , and the total Hilbert space is divided into two subspaces with even or odd numbers of Jordan-Wigner fermions. The different-parity states degenerate. We only treat the eigenstates $|\Psi_+\rangle$ in the even-parity sector ($H|\Psi_+\rangle = E|\Psi_+\rangle$, $P|\Psi_+\rangle = |\Psi_+\rangle$) in the main text. The operator R has the eigenvalues ± 1 (we shortly call it as R -parity), and can be efficiently used for identifying the eigenstates. The operator S corresponds to spin inversion, and the spectra are symmetric with respect to the negative and positive sides in a specific parity sector.

The Jordan-Wigner representation of the operator R is given by $R = \sigma_{C_1}^x \sigma_{C_2}^x = (f_{C_1}^\dagger - f_{C_1})(f_{C_2}^\dagger + f_{C_2})$. The eigenstates of R are summarized as follows:

$$R(|eeff\rangle \pm |efef\rangle) = \pm(|eeff\rangle \pm |efef\rangle), \quad (\text{A5})$$

$$R(|ffee\rangle \pm |feef\rangle) = \pm(|ffee\rangle \pm |feef\rangle), \quad (\text{A6})$$

$$R(|ffff\rangle \pm |feef\rangle) = \pm(|ffff\rangle \pm |feef\rangle), \quad (\text{A7})$$

$$R(|eeee\rangle \pm |effe\rangle) = \pm(|eeee\rangle \pm |effe\rangle), \quad (\text{A8})$$

where we take the duplicate signs in the same order. The general eigenstates in the even-parity sector can be represented as

$$|\Psi_+\rangle = a_1(|eeff\rangle + r|efef\rangle) + a_2(|ffff\rangle + r|feef\rangle) + \lambda a_1(|ffee\rangle + r|feef\rangle) + a_3(|eeee\rangle + r|effe\rangle), \quad (\text{A9})$$

where r ($= \pm 1$) is the eigenvalue of R , λ ($= \pm 1$) is the eigenvalue of space inversion, and parameters a_i ($i = 1, 2, 3$) are determined by solving $H|\Psi_+\rangle = E|\Psi_+\rangle$ and by the normalization condition (we do not explicitly introduce the space-inversion operator, since it is not easy to write it by the Pauli matrices).

Furthermore, we introduce the operator

$$Q\sigma_A^x = i\sigma_A^y \sigma_{C_1}^z \sigma_{C_2}^x. \quad (\text{A10})$$

This operator commutes with H for $h = 0$. A remarkable property of this operator is to satisfy $\{Q\sigma_A^x, R\} = 0$ and $[Q\sigma_A^x, P] = 0$. The state $Q\sigma_A^x|\Psi_+\rangle$ degenerates with $|\Psi_+\rangle$, but the eigenvalue of R for $Q\sigma_A^x|\Psi_+\rangle$ is different from that for $|\Psi_+\rangle$. Thus, R identifies the degeneracy at $h = 0$. Because of the R -parity change, we obtain

$$\langle \Psi_+ | Q\sigma_A^x | \Psi_+ \rangle = 0. \quad (\text{A11})$$

Appendix B: Derivation of ΔE_B^{\max} and $\Delta E_{B,B}^{\max}$

Let us derive the maximum of ΔE_B , ΔE_B^{\max} . For this purpose, we first transform ΔE_B into the following form:

$$\Delta E_B = \sqrt{W_0^2 + X_0^2} \cos(2\theta + \delta_0) - |W_0|, \quad (\text{B1})$$

where

$$W_0 = (1 - s_z^2) \epsilon_B + (1 - s_x^2) \epsilon_R, \quad (\text{B2})$$

$$X_0 = r_x s_y (kC_{AR} - hC_{AB}) + r_y s_x hD_{AB}, \quad (\text{B3})$$

and the phase factor δ_0 is determined by the following relations:

$$\cos \delta_0 = \frac{-W_0}{\sqrt{W_0^2 + X_0^2}}, \quad (\text{B4})$$

$$\sin \delta_0 = \frac{-X_0}{\sqrt{W_0^2 + X_0^2}}. \quad (\text{B5})$$

We find

$$\Delta E_B \leq \sqrt{W_0^2 + X_0^2} - |W_0|, \quad (\text{B6})$$

and ΔE_B^{\max} is obtained for $2\theta + \delta_0 = 0$. The RHS of Eq. (B6) is a function of \vec{r} and \vec{s} , which are determined to maximize ΔE_B . The factor W_0 is represented as

$$W_0 = \epsilon_B \sin^2 \xi + \epsilon_R (1 - \sin^2 \xi \cos^2 \eta). \quad (\text{B7})$$

According to Eq. (14), we find

$$kC_{AR} - hC_{AB} = -hD_{AB}, \quad (\text{B8})$$

and thus the factor X_0 is represented as

$$X_0 = (r_y s_x - r_x s_y) hD_{AB} = hD_{AB} \sin \mu \sin \xi \sin(\nu - \eta). \quad (\text{B9})$$

The RHS of Eq. (B6) is an increasing function of $\sin^2 \xi$, and is maximized for $\xi = \pi/2$. After that, we obtain $W_0 = \epsilon_B + \epsilon_R \sin^2 \eta$ and $X_0 = hD_{AB} \sin \mu \sin(\nu - \eta)$. The η dependence of X_0 can be absorbed by the optimization of ν , and thus, we can determine η to optimize W_0 . The RHS of Eq. (B6) is a decreasing function of $|W_0|$. Since ϵ_B and ϵ_R are negative, we take $\eta = 0$. The RHS of Eq. (B6) is an increasing function of $|X_0|$, and thus we take $\mu = \nu = \pi/2$. Finally, we obtain Eq. (41).

We also derive the maximum value of $\Delta E_{B,B}$, $\Delta E_{B,B}^{\max}$. For this purpose, we transform $\Delta E_{B,B}$ into the following form:

$$\Delta E_{B,B} = \sqrt{W^2 + X^2} \cos(2\theta + \delta) - |W|, \quad (\text{B10})$$

where

$$W = \epsilon_B (1 - s_z^2) = \epsilon_B \sin^2 \xi, \quad (\text{B11})$$

$$X = -h(r_x s_y C_{AB} - r_y s_x D_{AB}) = -4Z^2 h \sin \mu \sin \xi \{\sin(\eta - \nu) + \alpha \beta \sin(\eta + \nu)\}, \quad (\text{B12})$$

and the phase factor δ is determined from the the following relations:

$$\cos \delta = \frac{-W}{\sqrt{W^2 + X^2}}, \quad (\text{B13})$$

$$\sin \delta = \frac{-X}{\sqrt{W^2 + X^2}}. \quad (\text{B14})$$

We find

$$\Delta E_{B,B} \leq \sqrt{W^2 + X^2} - |W|, \quad (\text{B15})$$

and $\Delta E_{B,B}^{\max}$ is obtained for $2\theta + \delta = 0$. The RHS of Eq. (B15) is to be maximized with respect to \vec{r} and \vec{s} . The RHS of Eq. (B15) is an increasing function of $\sin^2 \xi$, and we take $\xi = \pi/2$. Then, the RHS of Eq. (B15) is maximized for the maximum value of $|X|$. We take $\mu = \eta = \pi/2$ and $\nu = 0$, since $\alpha\beta > 0$. Finally, we obtain Eq. (48).

Appendix C: Effect of degeneracy between even- and odd-parity states

In the main text, we focused on the lowest-energy state $|\psi\rangle$ in the even-parity sector. The state $|\psi\rangle$ degenerates with $|\phi\rangle = Q|\psi\rangle$ in the odd-parity sector. Here, we check whether our result holds in the odd-parity sector. For this purpose, we can use the following transformation $[P_A(n) = (I_A + n\vec{r} \cdot \vec{\sigma}_A)/2]$:

$$QP_A(n)Q = P_A(-n) \quad (r_z = 0), \quad (\text{C1})$$

$$QU_B(n)Q = U_B(n), \quad (\text{C2})$$

$$Q(ib_A b_B)Q = ib_A b_B, \quad (\text{C3})$$

$$Q(ic_A c_B)Q = ic_A c_B, \quad (\text{C4})$$

where $Qb_i Q = -b_i$ and $Qc_i Q = -c_i$ ($i = A, B$). We find

$$\langle \phi | ib_A b_B | \phi \rangle = \langle \psi | ib_A b_B | \psi \rangle, \quad (\text{C5})$$

$$\langle \phi | ic_A c_B | \phi \rangle = \langle \psi | ic_A c_B | \psi \rangle. \quad (\text{C6})$$

Thus, the b - and c -Majorana correlators are equivalent in both even- and odd-parity sectors. We also find that Q changes the sign of n in Eq. (C1). The QET performance at least for $r_z = 0$ is not affected by the parity change, since the sign change in Eq. (C1) can be absorbed by that of r_x and r_y .

It would be helpful for readers to mention four-fold degeneracy of the lowest-energy eigenstates for $h = 0$. The eigenstates are identified with the signs of the eigenvalues of P and R where the eigenvalue of P is denoted as p ($= \pm 1$). The eigenstates are specified as $|+, +\rangle = |\psi\rangle$, $|+, -\rangle = Q\sigma_A^x |\psi\rangle$, $|-, +\rangle = b_A |\psi\rangle$, and $|-, -\rangle = Q|\psi\rangle = |\phi\rangle$, where the two signs in $|\pm, \pm\rangle$ correspond to the signs of p and r from the left. Then, we find

$$\langle p, r | ib_A b_B | p, r \rangle = -pr C_{AB}, \quad (\text{C7})$$

$$\langle p, r | ic_A c_B | p, r \rangle = D_{AB}. \quad (\text{C8})$$

Therefore, at least for $h = 0$, the absolute values of the b - and c -Majorana correlators do not change for any combination of p and r .

Appendix D: On the minimization in Eq. (68)

We show some details about the minimization in Eq. (68). For general $P_A(n) = (I_A + n\vec{r} \cdot \vec{\sigma}_A)/2$, the reduced density matrix $\rho_B^m(n)$ is given by

$$\rho_B^m(n) = (1 - \theta) |e\rangle \langle e| + \kappa |e\rangle \langle f| + \kappa^* |f\rangle \langle e| + \theta |f\rangle \langle f|, \quad (\text{D1})$$

where θ and κ are respectively defined by

$$\theta = \frac{2Z^2 ((1 - nr_z) + \alpha^2 (1 + nr_z))}{1 + 2nr_z (\alpha^2 - \beta^2) Z^2}, \quad (\text{D2})$$

$$\kappa = \frac{2nZ^2 ((r_x + ir_y) + \alpha\beta (r_x - ir_y))}{1 + 2nr_z (\alpha^2 - \beta^2) Z^2}. \quad (\text{D3})$$

The eigenvalues of $\rho_B^m(n)$ are given by

$$\lambda_{\pm}^m(n) = \frac{1}{2} \left(1 \pm \sqrt{1 - 4\theta(1 - \theta) + 4|\kappa|^2} \right). \quad (\text{D4})$$

We find that $\lambda_{\pm}^m(n)$ depend on both of n and \vec{r} . Furthermore, we find

$$p_n = \frac{1}{2} (1 + 2nr_z (\alpha^2 - \beta^2) Z^2), \quad (\text{D5})$$

and p_n also depends on n . We examine $\sum_n p_n S(\rho_B^m(n))$ as functions of h/k and \vec{r} . We have confirmed numerically that $\sum_n p_n S(\rho_B^m(n))$ is minimized for $r_x = 1$. Therefore, it is reasonable to take $P_A(n) = (I_A + n\sigma_A^x)/2$.

Appendix E: Proof of equivalence between Eq. (48) and the RHS of Eq. (65) for optimized $P_A(n)$

The equivalence between Eq. (48) and the RHS of Eq. (65) for optimized $P_A(n)$ is derived by using β_{eff} that is a unique solution of Eq. (68).

For the derivation of β_{eff} , let us start with ρ_B^i and $\rho_B^m(n)$ that are respectively evaluated as

$$\rho_B^i = 2Z^2 [(1 + \beta^2) |e\rangle \langle e| + (1 + \alpha^2) |f\rangle \langle f|], \quad (\text{E1})$$

$$\rho_B^m(n) = 2Z^2 [(1 + \beta^2) |e\rangle \langle e| + (1 + \alpha^2) |f\rangle \langle f| + n(1 + \alpha\beta) (|e\rangle \langle f| + |f\rangle \langle e|)]. \quad (\text{E2})$$

A remarkable property of $\rho_B^m(n)$ is that the eigenvalues, λ_{\pm}^m , do not depend on n :

$$\lambda_{\pm}^m = \frac{1}{2} \left(1 \pm \sqrt{1 - 16Z^4 (\alpha - \beta)^2} \right) \equiv \frac{1}{2} (1 \pm g). \quad (\text{E3})$$

Thus, I_{QC} is simply represented as $I_{\text{QC}} = S(\rho_B^i) - S(\rho_B^m(n))$. Since λ_{\pm}^m is independent of n , Eq. (68) is reduced to $S(\sigma_B) = S(\rho_B^m(n))$ for the optimized $P_A(n)$. Then, we can solve Eq. (68) for β_{eff} by just comparing the eigenvalues of σ_B with λ_{\pm}^m . We find

$$\beta_{\text{eff}} h = \log \sqrt{\lambda_+^m / \lambda_-^m}. \quad (\text{E4})$$

Let us compare $\Delta E_{B,B}^{\max}$ in Eq. (48) with the RHS of Eq. (65). For this purpose, we transform the RHS into the following form:

$$\begin{aligned} & \mathcal{F}(\rho_B^i; H_B) - F(\sigma_B) + \frac{1}{\beta_{\text{eff}}} I_{\text{QC}} \\ &= \epsilon_B + \frac{h}{\log \sqrt{\lambda_+^{\text{m}}/\lambda_-^{\text{m}}}} (\log Z_{\text{eff}} - S(\rho_B^{\text{m}})), \end{aligned} \quad (\text{E5})$$

where the partition function is evaluated as $Z_{\text{eff}} =$

$\text{tr}_B e^{-\beta_{\text{eff}} H_B} = 1/\sqrt{\lambda_+^{\text{m}}\lambda_-^{\text{m}}}$. We can analytically show

$$\begin{aligned} & \sqrt{\left(\frac{\epsilon_B}{h}\right)^2 + C_{AB}^2} \\ &= \sqrt{\left(2Z^2(\alpha^2 - \beta^2)^2\right)^2 + (4Z^2(1 + \alpha\beta))^2} \\ &= 2Z^2 \sqrt{4 + 8\alpha\beta + (\alpha^2 + \beta^2)^2} \\ &= g, \end{aligned} \quad (\text{E6})$$

and

$$\begin{aligned} & \frac{\log Z_{\text{eff}} - S(\rho_B^{\text{m}}(n))}{\log \sqrt{\lambda_+^{\text{m}}/\lambda_-^{\text{m}}}} \\ &= \frac{-\log \sqrt{\lambda_+^{\text{m}}\lambda_-^{\text{m}}} + \lambda_+^{\text{m}} \log \lambda_+^{\text{m}} + \lambda_-^{\text{m}} \log \lambda_-^{\text{m}}}{\log \sqrt{\lambda_+^{\text{m}}/\lambda_-^{\text{m}}}} \\ &= \frac{-\log \sqrt{\lambda_+^{\text{m}}\lambda_-^{\text{m}}} + \frac{1}{2}(1+g) \log \lambda_+^{\text{m}} + \frac{1}{2}(1-g) \log \lambda_-^{\text{m}}}{\log \sqrt{\lambda_+^{\text{m}}/\lambda_-^{\text{m}}}} \\ &= g. \end{aligned} \quad (\text{E7})$$

Therefore, the equality between $\Delta E_{B,B}^{\max}$ in Eq. (48) and the RHS of Eq. (65) is confirmed by our optimized $P_A(n)$.